Nuclear Inst. and Methods in Physics Research, A 980 (2020) 164462

Contents lists available at ScienceDirect

Nuclear Inst. and Methods in Physics Research, A

journal homepage: www.elsevier.com/locate/nima

Hodoscope with Timepix detectors for PilsenCube2 cubesat

Ondřej Urban [a,*], Ondřej Vavroch [a], Libor Poláček [a], Vjačeslav Georgiev [a], Petr Burian [a,b], Pavel Turjanica [a], Pavel Fiala [a], Pavel Broulím [a], Benedikt Bergmann [b]

[a] Faculty of Electrical Engineering, University of West Bohemia, Univerzitní 26, Pilsen 312 00, Czech Republic
[b] Institute of Experimental and Applied Physics, Czech Technical University in Prague, Husova 240/5, 110 00 Prague, Czech Republic

ARTICLE INFO

Keywords:
Timepix
Cubesat
Hodoscope
Radiation
Spectroscopy
Space

ABSTRACT

The contribution describes the design of Timepix-based hodoscope for cubesat applications, such as PilsenCube2, developed by the University of West Bohemia. The hodoscope is composed of two Timepix detectors with silicon thickness of 300 μm, placed in back-to-back arrangement and rotated relative to each other by 90°, forming a telescope set-up. A copper separator is placed between two detectors to distinguish electrons and protons. The payload hardware and firmware are designed to support single detector operation as well as dual detector operation mode, in which particle coincidence detection is possible. The hodoscope electronic has been designed with respect to harsh radiation environment present in LEO (Low Earth Orbit). The device involves independent radiation hardened power supplies, including bias high voltage supply (up to 250 V) and auxiliary threshold reference DAC for each Timepix detector. Considering highly limited achievable data throughput between the CubeSat and the ground control station, advanced on-board data processing has been developed to reduce the size of transmitted data. The on-board data processing is provided by the radiation hardened SoC (System on Chip) Smartfusion2.

1. Introduction

One of the interesting applications of Timepix detectors is a spectroscopy of cosmic radiation. Several projects regarding this topic have already been carried out. Some of such projects are for example the spectroscope at the VZLUSAT-1 cubesat [1], the SATRAM spectroscope present at the Proba-V satellite [2], or the spectroscope at the RISESat [3]. However, none of such spectroscope boards implements on-board data processing, and thus the data frames (pixel matrices) have to be stored in the memory and when possible sent to the ground control station.

The main particles of interest in the near earth orbit are electrons in the range from 100 keV – 7 MeV and protons up to 400 MeV. While space radiation monitors based on diode stacks require shielding for the particle species separation, Timepix devices profit from the pixelation, which allows to use the characteristic imprints in the sensor matrix together with the stopping power information for the determination of the impacting particle type [4]. Thus, a radiation monitor of low mass (< 200 g) can be provided.

This hodoscope was designed to provide on-board data analysis using radiation hardened components, and thus to allow direct production of the measured spectra instead of saving the entire measured frames. Thanks to this on-board data processing the required data throughput between the pico-satellite and the ground control station is greatly reduced.

2. The pilsenCube2 project

The PilsenCube2 is pico satellite of the 1U category, which is being developed at the University Of West Bohemia in Pilsen. It is a successor of previously developed pico satellites PilsenCube [5,6] and VZLUSat –1 [7].

The main payloads of this cubesat shall be the hodoscope board, presented in this paper and various communication-related experiments. However the purpose of PilsenCube2 is not only to expand the experience gained with previous space related projects, but also to attract students to the scientific studies. Therefore it also carries payloads developed in collaboration with high school students, such as CMOS camera for visible wavelengths, infra-red camera, tester for evaluation of radiation tolerance of non-radiation hard MCUs and a 3-axis gyroscope.

The communication with the ground control station shall be realized using the UHF band. The data rate for the communication with the ground control station is only 4800 Bd. This data rate has been

* Corresponding author.
E-mail addresses: urbano@kae.zcu.cz (O. Urban), vavrocho@kae.zcu.cz (O. Vavroch), lpolacek@rice.zcu.cz (L. Poláček), georg@kae.zcu.cz (V. Georgiev), burianp@rice.zcu.cz (P. Burian), turjanic@rice.zcu.cz (P. Turjanica), pavelf@rice.zcu.cz (P. Fiala), broulimp@rice.zcu.cz (P. Broulím), benedikt.bergmann@utef.cvut.cz (B. Bergmann).

https://doi.org/10.1016/j.nima.2020.164462
Received 28 February 2020; Received in revised form 20 July 2020; Accepted 22 July 2020
Available online 4 August 2020
0168-9002/

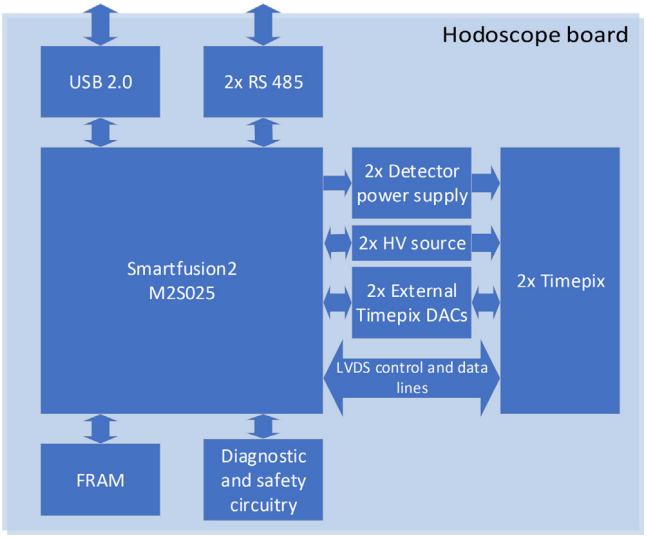

Fig. 1. Block diagram of the hodoscope board hardware.

successfully used in the VZLUSat −1 project. This allows download of approximately 260 kB of data per day [7].

3. Hardware features

The hodoscope board is mounted with two Timepix detectors, forming a telescope setup, where the detectors are back-to-back arranged and rotated by 90° to each other. Each detector has its own radiation hardened power supply, including an adjustable high voltage bias source providing up to 250 V. Radiation hardened FPGA SoC device (Microsemi Smartfusion2) is used for measurement control, data processing, current consumption measurement, temperature monitoring and power supplies control. The SoC device consists of a Cortex-M3 microprocessor, operating up to 166 MHz, 64 kB SRAM and 256 kB of embedded flash memory (eNVM) and an FPGA (Field-Programmable Gate Array) with 27, 696 LEs (Logic Elements). The schematic diagram of the hodoscope board can be seen in Fig. 1.

Previously published radiation tests of the Smartfusion2 SoC (e.g. [8–10]) show, that this device is robust to SEU and TID up to approximately dose of 500 Gy. This meets the requirements of platform considered for the low Earth orbit. The hodoscope uses three external FRAM (Ferroelectric RAM) memory devices providing 1.5 MB space in total for storage of configuration, calibration and measurement data. The photo of the hodoscope board prototype is shown in Fig. 2 with a view from the top side and from the bottom side of the board.

3.1. Timepix detector

This board uses two silicon Timepix detectors. The detector comprises of a detector layer with matrix of 256 x 256 pixels and an ASIC (Application Specific Integrated Circuit). Each pixel has a dimension of 55 x 55 μm and thus the total size of the detector is approximately 1.4 x 1.4 cm. The thickness of the pixel silicon used in this application is 300 μm. The detector can be operated in three modes: single particle counting, ToT (Time over Threshold) and ToA (Time of Arrival). In this particular application the ToT mode is used.

The Timepix chip readout is frame-based. This means that the entire frame measured during the exposition period is red out. The acquisition time of the Timepix sensor is controlled by external signal and is limited by specific application firmware. The only exception is the ToA mode where the acquisition time is limited by the Timepix counter overflow.

The energy resolution of the Timepix detector is usually stated as a sigma of the distribution measured while irradiating the detector by photons with the energy of 60 keV, and the typical value is around 2 keV

The Timepix detector's operating temperature limit is about 80 °C if the silicon detector layer is used. However the noise is more significant if the detector reaches such high temperatures. This temperature limit is still acceptable, compared for example with the Timepix chip with the CdTe detector layer, where the temperature limit is much lower and the detector has to be kept under approximately 50 °C. That is one of the reasons why the silicon detector layer has been chosen for this application.

The Timepix detector can operate with various bias voltages, depending on the detector layer thickness and type. In this case where 300 μm thick silicon detection layer is used, the usual bias voltage range is from 30 V to 90 V. For this case the bias voltage in the flight configuration shall be 40 V in order to prolong the charge collection compared with the higher bias settings and thus to prevent saturation of the pixels in case of high energy particles.

Table 1
Measured power consumption of the hodoscope board in different modes of operation.

Mode	Power consumption [W]
Measurement mode	1.789
Detectors OFF	1.002
Sleep mode	0.546

3.2. External DACs

The hodoscope board is equipped with two external DACs. These external digital to analog converters have two functions in this hodoscope board. The first purpose is for testing. Each pixel of the Timepix detector has can be connected to the external testing input through 8 fF capacitor. If the pixels functionality testing is required, the external DAC creates an impulse on these testing inputs and the pixel hit is simulated.

The other function of the DAC is an analog voltage backup. This feature might be useful in case of Timepix detector internal DAC failure, which would make the measurement impossible. In such case the Timepix can be configured to receive the analog signal from an input pin connected to these external DACs.

3.3. Communication interfaces

The developed device implements two communication interfaces. The first is the USB 2.0 interface used for debugging and calibration purposes.

For the communication with the cubesat's OBC (On-Board Computer) and the ground control station two RS485 buses are used. For this purpose a protocol for communication with the other cubesat modules has been developed. This protocol provides measurement control, data transmission and diagnostics and thus full control of the device is available through the RS485 buses. The second, duplicate RS485 bus is present for safety reasons (a backup of the main bus). The baud rate for communication between the OBC and other payloads is 250 kBd.

3.4. Power consumption

The hodoscope board is equipped with circuitry for power consumption measurement of the entire board and as well as for the individual detectors. This allows continuous monitoring of the power consumption and an eventual power shutdown in case of unexpected increase in the supply currents when a safety is jeopardized.

The power consumption of the entire hodoscope board equipped with two detector chips has been measured for different states of the device and results are shown in Table 1.

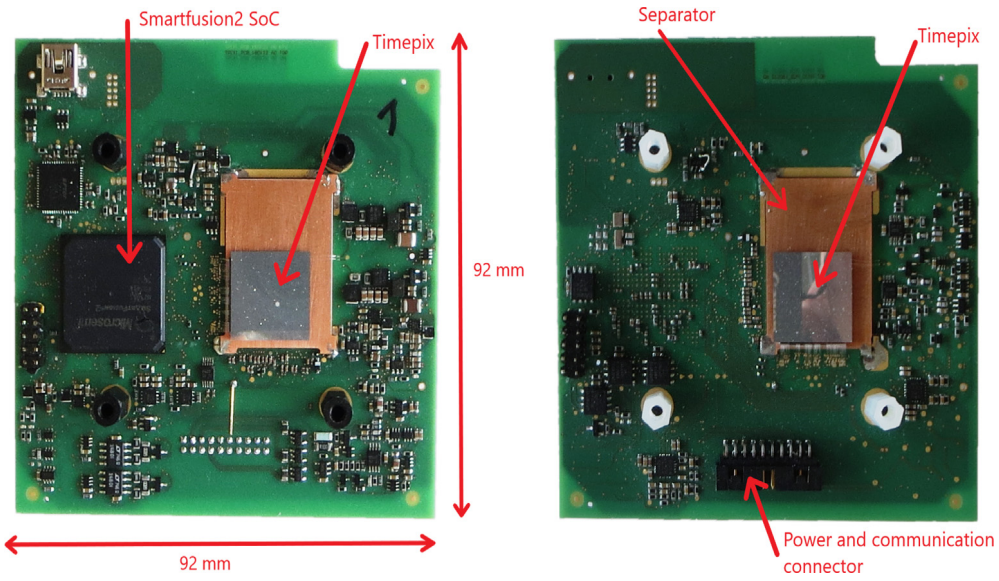

Fig. 2. Prototype of the hodoscope board (top and bottom view).

The power consumption during the measurement is dependent on clock frequency. In current setup the frequency for the Timepix chip has been set to 10 MHz (where the 100 MHz is the maximal frequency). This setting of the frequency setting provides sufficient ToT resolution, while keeping the power consumption relatively low. When the measurement is not active, the Timepix clock is disabled and thus the power consumption is lowered. Some techniques of Timepix detector power consumption optimization are also described in [11]

3.5. Electron separator

Each of the two Timepix detectors is mounted on a 2 mm thick copper layer. This means that any particle detected by both detectors has to pass total 4 mm of copper. This is only possible for particles with particularly high energies.

The main purpose of the separator is to separate low energy electrons from other high energy particles (mostly protons on LEO). The thickness of the separator has been chosen according to these requirements, and thus the range of electrons and protons in copper have been simulated. The results of the simulation using the "estar" and "pstar" software can be seen in Fig. 3.

One can see that for copper thickness of 4 mm the minimal energy, required for the protons to penetrate the separator is approximately 50 MeV. In case of electrons the minimal energy for penetration is above 5 MeV. While protons up to ~80 MeV can reliably be separated from electrons using the pattern recognition and pulse height (energy deposition) analysis, protons of energies >80 MeV, especially when hitting the sensor perpendicularly create a signal, which cannot be differentiated from an electron in a single layer. A background in the high energy proton channel could be produced by electrons >5 MeV. However, the fluxes of such highly energetic electrons are very low.

The separator plates also provide heat dissipation of the Timepix chip.

4. Automatic exposition time adjustment

One of the challenging points of the space radiation monitoring using the frame-based pixel detectors is the irregular distribution of the radiation intensity at the low Earth orbit. The overall particle hit rates at the LEO are expected to be approximately in the orders of 10^6 up to 10^{11}, as described in [8].

This may cause problems with the frame occupation, as the number of incident particles can vary greatly when the acquisition time is fixed. Too high frame occupancy causes the cluster overlapping and thus makes their analysis impossible.

The solution of this problem is the dynamic acquisition time adjustment according to the frame occupancy, as seen e.g. in the Timepix2 chip and the Katherine readout [12]. Unfortunately, there is no hardware support for this feature on the side of Timepix detector. For that reason this exposition adjustment has to be implemented by the control software.

The developed algorithm, providing an adjustment of the exposure time, is based on a PI (Proportional–Integral) regulator. In order to achieve optimal performance and stability over various incident particle fluxes the coefficients of the regulator are automatically adjusted. This adjustment is performed every measurement and is based on the ratio of the incident particles and the exposure time. Also the maximal regulation step is limited to avoid unexpected oscillations. The achieved results are displayed in Fig. 4. The upper graph shows number of hit pixels for both detectors for each subsequent acquired frame, while the lower graph shows frame acquisition time decrease as the regulator is trying to achieve the desired frame occupancy.

The behavior of the exposition time regulator has been tested using an X-ray tube while the required total occupancy (for both detectors) has been set to 5000 hits per frame. The measurement has been carried out for X-ray tube voltage of 30 kV and four different currents (5 μA to 75 μA). In order to test the response of the regulator in extreme conditions, the X-ray tube has been switched on while the exposure time has been at its maximum (0.1 s) due to the saturation of the regulator. One can observe that for all current settings the regulator is able to achieve the required occupancy within approximately 8 measurements and is stable over wide ranges of target exposition time. The minimal exposition time is limited by the firmware capabilities and is 1 us. This minimal exposure time limits the effectiveness of the exposure time regulation and may lead to over-occupancy if the particle fluxes are particularly high.

5. Hodoscope commands

In order to ensure setup, control and diagnostic of the hodoscope board, various command handling have been implemented in the hodoscope software. The hodoscope board is always in a role of a slave and only responses when requested. These commands are received by the board via RS485 interface and ensure following features of the device:

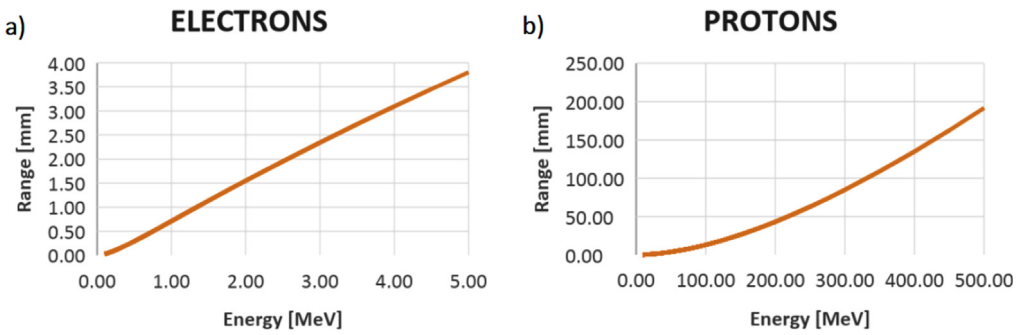

Fig. 3. Simulation results of the electron and proton range in copper.

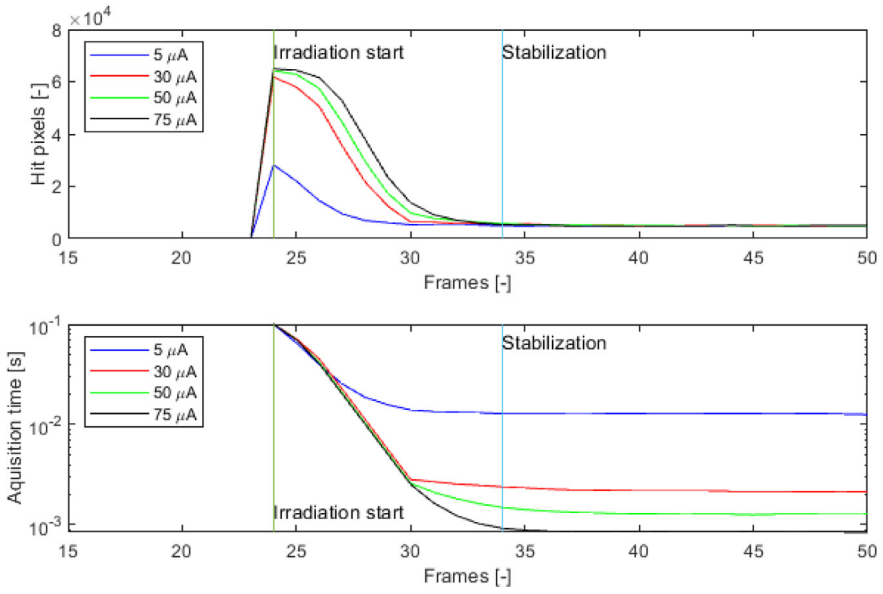

Fig. 4. Measured reaction of the exposition time regulator to an X-ray exposure for various X-ray tube currents.

- Upload new code image for execution (original image is preserved)
- Change image for execution (original or newly uploaded)
- Get diagnostic data (board temperature, currents, voltages)
- Set parameters for measurement (bias, threshold, exposition time limits)
- Start/abort measurement cycle
- Store entire frame
- Download spectrum (all spectra at once or specific spectrum only)
- Download entire frame
- Null the measured spectra

This protocol has been designed in order to provide universal hodoscope control either from PC control software, OBC, or any other master, connected via the RS485 bus.

6. Data processing

As already mentioned the throughput of the communication between the cubesat at the low Earth orbit and the ground control station is limited. The limits are caused by limited visibility of the satellite from the ground station receiver and by parameters of the transmission. Therefore, as much on-board data processing as possible is required to minimize the data size for transmission. Due to the limited computational power of Cortex-M3 platform (especially long access time of the FRAM memory), very careful optimization of used techniques and algorithms was fundamental demand.

When it comes to the download of the measurement data from the cubesat, three possibilities were taken in mind. The simplest method of data download is transmission of the entire frames, while using some kind of data compression (Lempel–Ziv-Welch 84 algorithm has been considered). Other possible way is transmission of the pixel hit energies and addresses within the matrix. The third possibility is to process the data and produce the resulting spectra on-board. With direct spectra production the data size for transmission is always fixed and depends on the number of spectra bins.

In the graph Fig. 5 comparison between spectrum transmission (considering 32 kB buffer for the spectrum) and other possibilities of the measured data transmissions (considering both detectors) is visualized. It can be seen that the spectra transmission is more convenient for frame occupancies greater than 6% even for single measurement.

Since the spectra production enables (and is intended for) storing data from multiple measurements (the amount of measurements between data transmissions is limited by maximum number of hits in the highest peak of the spectrum), the saved data size is even greater.

6.1. Cluster analysis

The first step of the data post-processing is the cluster analysis. Clusters are representation of sets of neighboring pixels detected at the same moment (within a defined time window). The cluster corresponds to a particle interacting in the sensor layer. The cluster analysis finds individual clusters in the frame and stores their fundamental features for further processing. Because of the large size of each frame (256×256

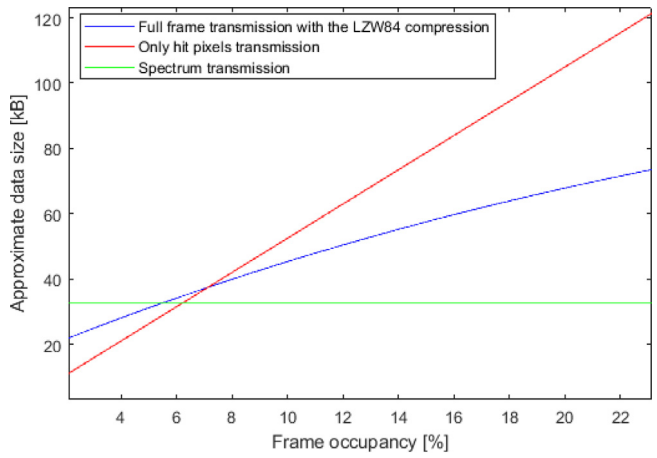

Fig. 5. Comparison between spectra size and other possible ways of data transmission for single measurement (using both detectors).

pixels, 14 bit/pixels) the frame cannot be analyzed at once, because the RAM memory is not big enough to store the entire frame. Therefore each line of pixels is processed separately and thus the memory requirements are decreased while providing the same results. The approach is also used in [6].

This technique of memory usage optimization is very convenient as it only has small influence on the frame processing time. The computation time of both single-line processing and full frame processing has been measured several times using implementation in the PC (since it is impossible to implement full frame processing using actual hodoscope hardware) to get the approximate ratio between these methods. The average measured time ratio between these approaches has been 1.07. The measured ratio of the two analysis approaches is expected to be almost similar when the actual hodoscope hardware with the Smartfusion2 SoC is used, and thus it is assumed that the line-by-line processing does not significantly reduce the analysis speed.

The information about individual clusters has to be stored in the memory for the entire data processing. Therefore the number of clusters within a frame has to be kept at reasonable level. Current version of the hodoscope board has a capability to store information 512 clusters per one detector. Once this level is reached the analysis is no longer possible and the following clusters are ignored. Also the maximal number of stored pixels is limited. This limitation is however not so problematic due to much smaller memory requirement for pixel storage (up to 8000 pixels per detector can be stored).

6.2. Cluster classification

After the clusters are identified, it is very convenient to sort them according to their physical properties into several categories:

- Dot (gamma, X-ray)
- Small blob (alpha, proton with 90° incident angle)
- Heavy blob (alpha, ion, proton with 90° incident angle)
- Straight track (minimum ionizing particle, electron)
- Heavy track (proton, ion)
- Curly track (electron)

In the picture above samples of typical cluster types captured with the prototype of the hodoscope device are shown.

This classification can be used to store spectra of each physical type separately. This can be convenient for the results evaluation, as the end user can simply download only desired spectra from the cubesat. Also the expected energy range for these physical types can be more precisely estimated and thus more efficient binning can be applied.

The first step in cluster classification is determination whether the cluster is the "dot" type, which is caused by gamma or X-ray radiation. The reason why it is convenient to perform this as a first step is that even though small detection efficiency at higher energies it is expected that the "dot" type cluster count shall be very significant. Moreover, the topology of such clusters is very simple (mostly a single pixel hit) and thus it is not necessary to perform further analysis and the cluster and the classification is finished if the cluster size and its energy is within specified range (single pixel events with particularly high energies are most likely to be caused by SEU and thus the energy has to be checked as well to exclude these events from regular spectra).

For other cluster types recognition additional parameters calculation is needed. The clusters of the "blob" type are well defined by their roundness. However this parameter might not be conclusive enough for "small blobs" since these can be only a few pixels in diameter. Therefore except the shape properties of these small clusters also the energy distribution within the cluster center is evaluated. This has been tested as very reliable way of classification since the clusters of the "small blob" type have the energy peak within the center of the cluster (if the volcano effect is not present).

If the cluster does not meet the requirements for the "small blob" or "heavy blob", the "heavy track" type cluster type is the next candidate for evaluation. These clusters are specified by their relatively big ratio of the inner pixel number to the total number of cluster pixels and an elliptic to straight shape (as shown in Fig. 6).

The last two classification categories are "straight track" and "curly track". The key criterion for the "straight track" classification is the number of in-line pixels and its ratio to the number of total pixels.

If none of the cluster types are successfully recognized, the type is set to "curly track". This type of track (typically caused by beta particles) has very variable shape and thus is automatically assumed when the requirements for other cluster types are not met.

6.3. The coincidence evaluation

Thanks to the telescope arrangement of the detectors the coincidence evaluation is possible. This allows us to identify high energy particles, penetrative enough to pass both copper separator plates.

For the coincidence evaluation the particle physical type is used to exclude the clusters that are unlikely to be caused by the same particle (e.g. blob in one layer and track in the other). Then the mutual position of the clusters is compared. In case of straight and heavy tracks the angle of particle impact and angle of rotation are also evaluated and compared with the other cluster.

The fact that the particle penetrated both detector layers can be used for further separation of such events from the output spectra and thus to provide more flexibility, as the data related to coinciding particles are stored separately.

6.4. Measurement outputs

The results of the entire cluster analysis are cluster type and its energy. The cluster energy is added to the appropriate spectrum according to its classification. The spectra are stored in the external FRAM memory. One of the important features of the FRAM memories (besides its radiation tolerance) is the non-volatility, which prevents the data loss in case of power outage.

Sometimes it might be important for the user to see the raw measured data. In this case the possibility to store the entire measured frame is implemented using special command from the OBC.

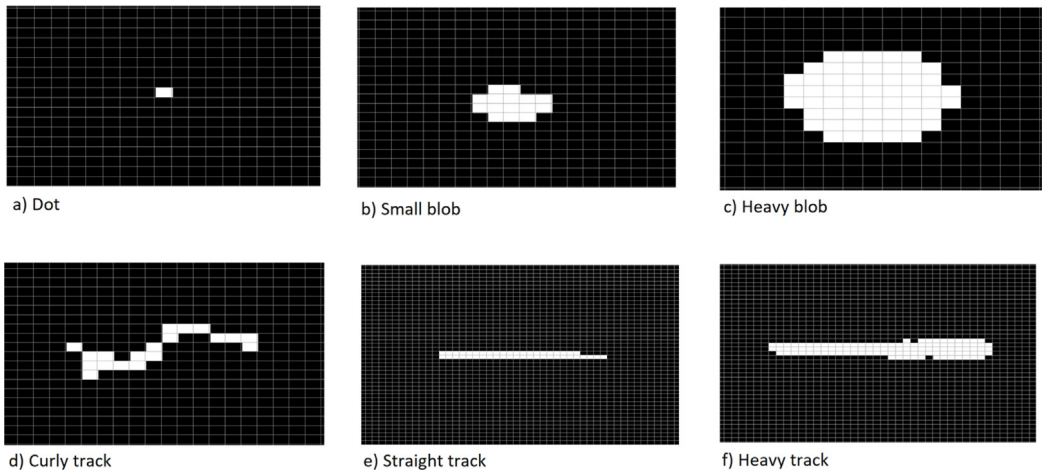

Fig. 6. Visualization of the typical cluster types measured with the Timepix detector.

Table 2
Particle classification results for 241-Am sources with and without alpha particle filter.

Particle type	241-Am with alpha separator	241-Am
Number of frames	247	456
Dot	93831	6851
Small blob	0	41760
Heavy blob	0	1290
Curly track	523	5632
Straight track	105	191
Heavy track	0	0

Table 3
The measured cluster types at the 3 He beam within 608 frames with 10 ms exposure time and 60° impact angle.

Particle type	Number of detected particles	Percentage of total particles
Dot	3145	13.05%
Small blob	551	2.28%
Heavy blob	5592	23.2%
Curly track	4209	17.46%
Straight track	5162	21.42%
Heavy track	5440	22.57%

7. Example of the on-board processing

In order to demonstrate the data processing capabilities of the device, a set of measurements has been carried out. The first two measurements have been done while irradiating the detectors by 9.5 kBq 241-Am source and a 300 kBq 241-Am source with alpha particle filter in order to achieve pure gamma X-ray radiation.

The measured data were analyzed using the on-board cluster processing algorithm in order to classify the captured clusters. The achieved results are presented in Table 2.

It can be observed that in case of the X-ray and gamma 241-Am source the clusters are identified without any problems. In case of 241-Am source without any alpha particle separator the identified particle types varied. When considering expected particle types achieved by X-ray, gamma and alpha decay of the 241-Am, it has been expected that the measured particle types shall be of "small blob", "heavy blob" and "dot" types. However the "curly track" types are present in considerable amount. This has several reasons. The first reason is that some particles hit the detector layer at the edge and therefore the shape is greatly distorted. The other reason is presence of "dead pixels" of the detector. These pixels are present naturally due to imperfect manufacturing process and due to possible damage to the electronic caused by irradiation. If such "dead pixel" is present within the cluster of smaller dimensions such, the classification may be incorrect.

The third measurement has been carried out on a cyclotron facility at the ÚJV Řež, a.s. The cyclotron has been used to accelerate ^{3}He ions to the energy of 16 MeV. From the visualization of the raw data from the hodoscope detectors and the Timepix3 with Katherine readout which has been present at the measurement as well it has been observed, that alongside the ^{3}He ions also lower energy particles were present. The raw frame captured by one of the hodoscope board detector is shown Fig. 7.

The measurement has been carried out with 40 V bias voltage and the exposure time was set manually to 10 ms.

Since the measurement has been carried out for the angle of 60° it is expected that the high energy ions shall be identified as the "heavy tracks" and the lower energy particles present alongside the ions as the "straight tracks". Also fair amount of "dot" clusters is expected as gamma radiation is present at the beam.

The results of the analysis are shown in Table 3.

From the results it can be observed, that the analysis also identified great amount of "heavy blob" cluster types. This is caused due to relatively good circularity of some of the incident ions. Also a lot of curly tracks is present as scattered particles from ion collisions with the surrounding material.

7.1. The measured spectrum of the He beam

The measured data has been analyzed using the on-board processing algorithm and the spectrum for "blob" types and "track" types has been measured. The resulting spectrum is shown in the picture Fig. 8. The measurement has been carried out in a ToT (Time over Threshold) mode.

It can be observed that the peak of the incident ions is easily distinguished. Also the fact that "curly tracks" and "dots" were not involved into the spectrum enabled better binning setting, in this case to 150 ToT.

7.2. Effect of the cluster overlapping

The problem of cluster overlapping has been mentioned in the chapter 4. In this chapter an example of such problem shall be shown for a measurement of a 241-Am. In this measurement the exposure time has been increased from relatively suitable time to higher acquisition time where the cluster overlapping has been observed more frequently and caused additional peak in the spectrum.

In case of the alpha particle cluster merge the resulting cluster shape is recognized as a heavy track. Table 4 shows the occurrence of the

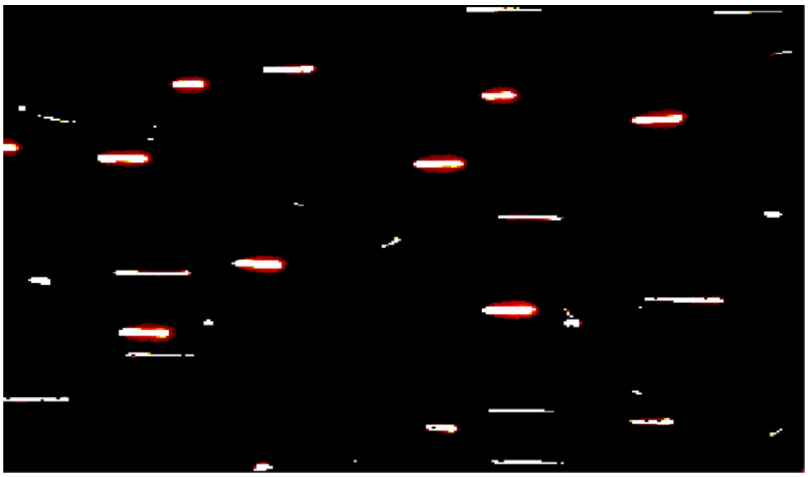

Fig. 7. Frame captured during measurement at the ^{3}He beam. The angle of detector to the beam has been 60°, the exposure time 10 ms and the bias voltage has been set to 40 V.

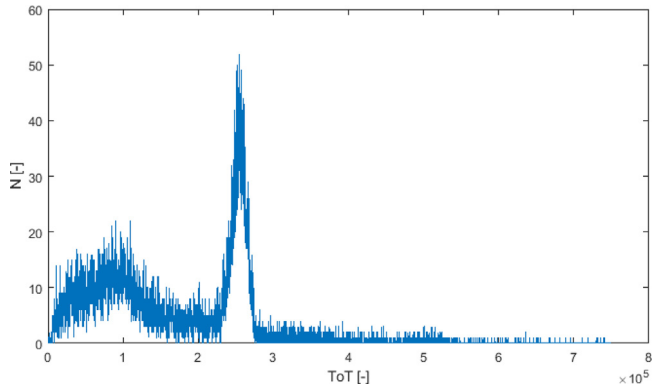

Fig. 8. The ToT spectrum measured at the ^{3}He beam with the energy of 16 MeV under the angle of impact 60°.

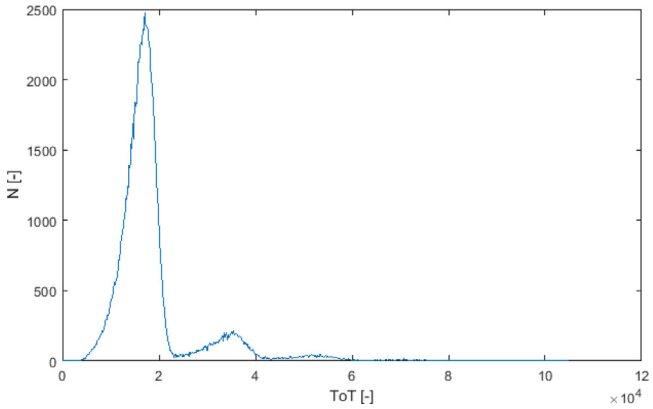

Fig. 9. The ToT spectrum of alpha particles emitted by 241-Am with 4 s exposure time. Second peak caused by cluster overlapping can be seen.

Table 4
The percentage of overlapping clusters for different exposure times while irradiating with the 241-Am source.

Acquisition time	Percentage of the overlapping clusters
1 s	0.37%
2 s	1.03%
3 s	1.63%
4 s	2.6%

heavy tracks caused by cluster overlapping for different acquisition times.

The effect on the resulting ToT spectrum is shown in the Fig. 9. It can be observed that there is a second peak with approximately twice as high ToT mean value.

8. Conclusion

The presented device is good solution for the radiation field monitoring and recognition in small satellite missions. It implements both low-level data processing (FPGA part of the device) and high-level processing based on the low level results (MCU part), which allows a direct production of measured data spectra. The board can be easily integrated as a payload for pico-satellites or similar applications. The hodoscope is controlled using RS485 bus via control/status commands from the satellite OBC. The designed firmware offers wide range of tools for data evaluation that makes it possible to modify the system for specific mission.

Declaration of competing interest

The authors declare that they have no known competing financial interests or personal relationships that could have appeared to influence the work reported in this paper.

Acknowledgments

This research was supported by the projects Engineering Applications of Microworld Physics (CZ.02.1.01/0.0/0.0/16_019/0000766), Research Infrastructure for CERN experiments (LM2015058) and Microworld Research in the frame of CERN infrastructure (LTT17018).

References

[1] Tomáš Báča, Michal Platkevič, Jan Jakubek, Veronika Stehlíková, Martin Urban, Ondrej Nentvich, Martin Blažek, Randall Mcentaffer, Vladimír Dániel, Adolf Inneman, Miniaturized X-ray telescope for VZLUSAT-1 nanosatellite with timepix detector, J. Instrum. 11 (2016) C10007, http://dx.doi.org/10.1088/1748-0221/11/10/C10007.

[2] C. Granja, S. Polansky, Z. Vykydal, S. Pospisil, A. Owens, Z. Kozacek, K. Mellab, M. Simcak, The SATRAM timepix spacecraft payload in open space on board the Proba-V satellite for wide range radiation monitoring in LEO orbit, Planet. Space Sci. (ISSN: 0032-0633) 125 (2016) 114–129.

[3] Robert Filgas, Milan Malich, Toshinori Kuwahara, Jan Broulim, Michael Holik, Morokot Sakal, Yu Murata, Hannah Tomio, Stefan Gohl, T. Johan, RISEPix—A Timepix-based radiation monitor telescope onboard the RISESAT satellite, Astron. Nachr. 340 (2019) 674–680, http://dx.doi.org/10.1002/asna.201913674.

[4] Stefan Gohl, Benedikt Bergmann, Hugh Evans, Petteri Nieminen, Alan Owens, Stanislav Posipsil, Study of the radiation fields in LEO with the space application of timepix radiation monitor (SATRAM), Adv. Space Res. (ISSN: 0273-1177) 63 (5) (2019) 1646–1660.

[5] P. Fiala, A. Voborník, Embedded microcontroller system for PilsenCUBE picosatellite, in: 2013 IEEE 16th International Symposium on Design and Diagnostics of Electronic Circuits & Systems (DDECS), Karlovy Vary, 2013, pp. 131–134, http://dx.doi.org/10.1109/DDECS.2013.6549804.

[6] R. Linhart, A. Voborník, I. Veřtát, Communication subsystem for PilsenCUBE nanosatellite, in: 2018 International Conference on Applied Electronics (AE), Pilsen, 2018, pp. 1–4, http://dx.doi.org/10.23919/AE.2018.8501441.

[7] I. Vertat, R. L. Inhart, M. Pokorny, J. Masopust, P. Fiala, J. Mraz, Small satellite ground station in pilsen — experiences with vzlusat-1 commanding and future modifications toward open reference ground station solution, in: 2018 28th International Conference Radioelektronika (RADIOELEKTRONIKA), Prague, 2018, pp. 1–6, http://dx.doi.org/10.1109/RADIOELEK.2018.8376393.

[8] Microsemi Corporation, IGLOO2 and SmartFusion2 65 nm Commercial Flash FPGAs 21 October 2014, 2014, [Online]. Available: https://www.microsemi.com/document-portal/cat_view/56661-internal-documents/56758-soc/56765-radiation-tid-reports.

[9] S. Danzeca, G. Tsiligiannis, SmartFusion2 and Artyx7 radiation test results for the new developments, in: TWEPP, 2017.

[10] Durwyn Dsilva, Jih-Jong Wang, Nadia Rezzak, Narayan Jat, Neutron SEE Testing of the 65 nm SmartFusion2 Flash-Based FPGA, 2015, pp. 1–5, http://dx.doi.org/10.1109/REDW.2015.7336722.

[11] P. Burian, P. Broulím, B. Bergmann, Study of power consumption of timepix3 detector, J. Instrum. 14 (2019) C01001–C01001. http://dx.doi.org/10.1088/1748-0221/14/01/C01001.

[12] P. Burian, P. Broulím, M. Jára, V. Georgiev, B. Bergmann, Katherine: ethernet embedded readout interface for Timepix3, J. Instrum. 12 (2017) C11001–C11001. http://dx.doi.org/10.1088/1748-0221/12/11/C11001.